IEEE Access
Multidisciplinary | Rapid Review | Open Access Journal

Received February 12, 2019, accepted March 18, 2019, date of publication March 26, 2019, date of current version April 8, 2019.

Digital Object Identifier 10.1109/ACCESS.2019.2906885

Self-Identification Respiratory Disorder Based on Continuous Wave Radar Sensor System

NGUYEN THI PHUOC VAN[1,4], (Student Member, IEEE), LIQIONG TANG[1], AMARDEEP SINGH[1], NGUYEN DUC MINH[2], SUBHAS CHANDRA MUKHOPADHYAY[3], (Fellow, IEEE), AND SYED FARAZ HASAN[1]

[1]School of Engineering and Advanced Technology, Massey University, Manawatu 4442 , New Zealand
[2]School of Electronics and Telecommunications, Hanoi University of Science and Technology, Hanoi 10000, Vietnam
[3]School of Engineering, Macquarie University, Sydney, NSW 2113, Australia
[4]Hanoi University of Industry, Hanoi 10000, Vietnam

Corresponding author: Nguyen Thi Phuoc Van (v.nguyen@massey.ac.nz)

This work was supported in part by the New Zealand Aid Program, New Zealand Ministry of Foreign Affairs and Trade, and in part by the Faculty for the Future Program, Schlumberger Foundation.

ABSTRACT Contactless vital signs detection, based on the Doppler radar sensor system, has opened a great opportunity in biomedical applications. The radar sensor system can be used to provide the respiratory information of people without disturbing their comfort. This sensor system promises high accuracy in measuring breathing disorders as it escapes the touching sensors which might cause discomfort to the user and negatively affect their sleeping habits. Moreover, this sensor system does not require any special environment or depend on temperature and light conditions. In this paper, we propose a model to the end users; this model is to be built based on neural networks. Our proposed system can diagnose whether a person has a low, normal, or high breathing rate. This model can also be extended to more specific categories to help doctors to determine breathing disorders in patients. In this paper, a continuous wave radar sensor system, based on a vector network analyzer (VNA), is used to measure the breathing rate remotely. The measured signal from this radar sensor system is then processed for further purposes. Different extracted feature methods are implemented to obtain the breathing rate from the non-contact radar sensor system. A model based on the machine learning technique is investigated to classify the breathing disorder. A total of 31 people who were asked to perform low/normal/high breathing were measured by the *CW* radar sensor. The measured data were also used to build a machine learning based model. The breathing rate measured by the *CW* radar sensor system is compared with the reference measurement by the five-point touching Shimmer sensor. The results of the breathing rate are compatible. Two main time–frequency (*TF*) extraction feature methods, short-time Fourier transform (STFT) and continuous wavelet transform (CWT), were implemented in the proposed system. Under these extraction techniques, some classification approaches were employed and have shown high accuracy in categorizing the respiratory types. The research shows the possibility of building an artificial intelligence (AI) module for a non-contact radar sensor system to inform the end user of their breathing situation. This research enables a smarter and more friendly remote-detecting vital signs sensor system.

INDEX TERMS Machine learning, vital signs detection, neuron network, classification problem.

I. INTRODUCTION

The first Doppler radar sensor system was used for medical application in the 1970*s* [1]. This system operated at 10 *GHz* frequency. Its function was very simple, in that an alarm was introduced when there was no breathing signal from a patient within 10 seconds for infants, and 30 seconds for adults. In the same vein, there are many studies which concentrate on the biomedical implementations of the radar sensor system [2]–[7]. The invention in [2] describes a non-acoustic pulse-echo radar used to detect movements of organs like heart, lung, arteries and so on. Inspired by sensor networks

The associate editor coordinating the review of this manuscript and approving it for publication was Qingxue Zhang.

for health care, Carlos [3] presents a dual function ultra-wide-band (*UWB*) technique for the radar sensor system. This system can act as a microwave Doppler radar to measure the heartbeat, and a sensor node to transfer heart information to the central block. This "duo" feature (monitoring and sharing data) of the sensor can function as an ideal node in body sensor networks. In line with Carlos's study [3], Ernestina *et al.* [4] discusses in more detail the feasibility of a vital signs detection radar sensor system, called frequency modulation - ultra wide band (FM-UWB) radar. This system integrated the advantages of *FM* radar and *UWB* radar in a single device. The most impressive features of Ernestina *et al.* are sensing vital signs (penetration, location, breathing rate, and heartbeat) and communicating to another node. However, this work did not establish any hardware prototype for the $FM - UWB$ system.

Later, in 2011, the *UWB* system-on-chip Radar sensor in 90 *nm* CMOS technology was investigated by Domenico Zito *et al.* [5]. Their on-chip device could observe the heart beat and respiration of adults and babies. This work enabled the continuous monitoring of the baby's breathing rate. Moreover, it gave high accuracy of measurement within a distance of 50 cm. This factor allowed more applications like respiratory disorder diagnosed purposes, or a warning to drowsy drivers. Different types of micro radar systems for medical, animal, and structural monitoring applications were reviewed by Stefano *et al*. [6], [8] in 2016 and 2017, respectively. These surveys carefully considered continuous wave (CW) radar, FM, UWB, and hybrid radar systems. The latter work focused on the short-range application of radar sensors. In the reference [7] Changzhan Gu *et al*. proposed a Doppler radar system with a digital post-distortion (DPoD) method to compensate for signal distortions and enhance the detecting accuracy of the radar system. Recently, Christoph *et al.* [9] investigated the physiological effects of the vital signs measurement of the radar sensor system. They discovered the cardiovascular system and the influence of antennae characteristics to the radar signal. The respiratory detection capability of the radar sensor is utilized in [10] to improve the safety for a driver. In this patent, the radar sensor system was combined with other systems, like processors, to monitor the respiratory system of a driver properly. Obviously, previous authors have made a great contribution to the vital signs detecting remote radar sensing system in terms of hardware and signal processing development. However, to the best knowledge of the authors, no-one has built the *AI* based model for this system.

To make the radar sensor system more intelligent, in this study, the specific machine learning model for the breathing sign detection radar is utilized to diagnose the respiratory disorder of the end user. Based on the training data set, the proposed system can give the medical information to a person, such as whether they have a high/low/normal breathing rate. This kind of warning is useful for the person to go further in checking out health problems. Moreover, the model could be extended to diagnose different types of respiratory disorders.

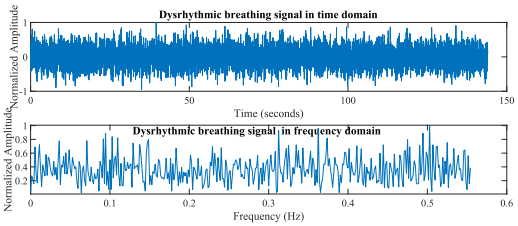

FIGURE 1. Simulation for dysthymic respiration.

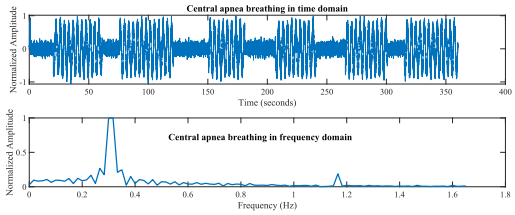

FIGURE 2. Simulation of cheyne stokes respiration signal.

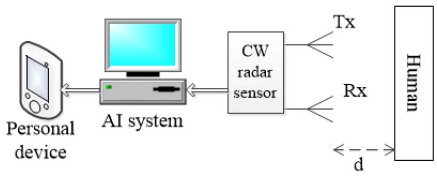

FIGURE 3. Block diagram.

For example, a person has dysrhythmic breathing problem when their respiratory has irregular rhythm of rate and amplitude. This type of breathing problem relates to a brain stem issue. The rhythm and amplitude of this type changes with the time, and it is difficult to estimate the breathing rate of a person who has this breathing disorder [11] (see Figure 1). Another example of breathing disorder is the central apnoea respiration. This problem occurs when a person's breathing stops for a duration lasting from 10 to 30 seconds. The apnoea duration corresponds with the time that the brain stops sending signals to the breathing control muscles [12]. Two above examples show that the breathing disorder can not be classified by simply estimating the peak frequency spectrum of receiving signal. Therefore, machine learning technique should be used to diagnose breathing disorder issues. In addition, this work collected data from 31 people when they perform high/low/normal respiration by *CW* radar sensor. This work assists further research in the field by publishing our data set.

This paper is structured as follows. Section II presents the discussion on proposed system diagram and functions of each module in the proposed system. Section III describes the experimental setup and Section IV gives discussion on measurement results. The final Section V is the conclusion and consideration for future work.

II. PROPOSED SYSTEM

The block diagram of the proposed system is presented in Figure 3. The system consists of three main modules,

a radar sensor, an *AI* module, and a personal device. A continuous wave (*CW*) is sent toward the human position through the transmitting antenna of *CW* radar sensor, the reflected signal from the human chest goes back to the sensor system through receiving antenna. The arctangent modulation is applied to the sensor system; the output signal at the sensor is proportional with the chest displacement. This signal is sampled at a frequency of 256 *Hz* before sending to *AI* module. At the *AI* module, signals are processed to provide useful information to the person through their personal devices.

A. OPERATING PRINCIPLE OF CW RADAR SENSOR

In the CW radar sensor, a single sin wave is transmitted toward the human position. Neglecting the amplitude, the transmitting signal is given as follows [13], [14].

$$Y_T = \cos\left(2\pi ft + \phi\left(t\right)\right) \tag{1}$$

where f is the operating frequency of radar sensor and $\phi\left(t\right)$ is the phase noise. When the transmitting signal reaches the chest of the person, this signal is then modulated by the displacement of the chest and reflects back to the receiving antenna of the sensor [13], [14]. The receiving signal can be written as:

$$Y_R = \cos\left(2\pi ft - \frac{4\pi d}{\lambda} - \frac{4\pi x\left(t\right)}{\lambda} + \phi\left(t - \frac{2d}{c}\right)\right) \tag{2}$$

where d is the distance from the sensor to the human location, λ is the wavelength of the sending signal, $x(t)$ is the chest displacement of the human, and c is the speed of light. The receiving signal is then down converted into the intermediate frequency (*IF*) signal. Two mixers are used in the down converter to get in phase (I) and quadrature (Q)signals. At the base band I and Q discrete signals are given as [15]:

$$B_I(n) \approx \cos\left[\theta + \frac{4\pi x(n)}{\lambda} + \triangle\phi(n)\right] \tag{3}$$

$$B_Q(n) \approx \sin\left[\theta + \frac{4\pi x(n)}{\lambda} + \triangle\phi(n)\right] \tag{4}$$

where θ is the constant phase shift due to the distance from the human position to the radar, and $\triangle\phi(t)$ is the phase noise. At the receiver, the arctangent demodulation is applied and the output signal of the radar sensor system can be calculated as

$$\psi(n) = arctan\left[\frac{B_Q(n)}{B_I(n)}\right] = \theta + \frac{4\pi x(n)}{\lambda} + \triangle\phi(n) \tag{5}$$

The output signal $\psi(n)$ of the radar sensor is processed by the *AI* module to extract the breathing rate and classify the breathing problems.

B. AI MODULE

The framework of the AI module is presented in Figure. 4. AI module consists of three main steps; data processing, feature extraction and classification. All the steps are implemented using Matlab *R2018b* on Intel Core *i5*, 16 *GB* memory configuration hardware running with Windows 7 *OS*.

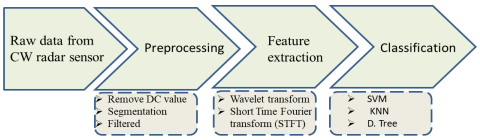

FIGURE 4. The steps implemented in the AI module.

In this module, the raw signal is reprocessed to remove the *DC* value and be filtered by an appropriated filter. The next step is to extract features based on time frequency technique. Finally, data is classified into different categories.

1) DATA PREPROCESSING AND FEATURE EXTRACTION

After visual inspection, five-minute data (i.e. 76800 data points because of 256 sampling rate) was extracted from the six minutes recording. Firstly, the *DC* value of the measure data was removed. The data was further bandpass filtered by [0.1 to 2] *Hz* Butterworth. We used the two most popular time-frequency (TF) methods [16]: short time Fourier transform (*STFT*) and continuous wavelet transform (*CWT*) to extract time-varying spectral properties of the breathing signal as our features for the classification model. *TF* features are used for classification and also give an instantaneous breathing rate of the user in the time domain.

In the *STFT*, first, a whole signal is divided into portions of equal window size, then subsequently applied the Fourier Transform (*FT*) on each portion, respectively [17]. The *STFT* $F(\tau, \omega)$ of the measured signal $\psi(t)$ is defined as:

$$F(\tau, \omega) = \sum_{-\infty}^{\infty} \psi(n)h(n-\tau)e^{-j\omega n} \tag{6}$$

where $h(n-\tau)$ is a window function. Based on Equation. 6, the power spectrum density (*PSD*) of the signal is determined as

$$P_S(\tau, \omega) = |F(\tau, \omega)|^2 \tag{7}$$

Above equations interpret that *FT* of each portion is captured with the window moves along the time axis of the entire signal. Correspondingly, $P_S(\tau, \omega)$ is a two-dimensional vector that stores power of the input signal according to time and frequency. *PSD* of *STFT* has a fixed resolution, because the width of window function is constant for all segments of input signal. Specifically, a wider window function brings a better frequency resolution, while a better time resolution [17] is brought about by narrow size of window function.

CWT is an alternative feature extraction method to get *TF* of a signal. This signal processing technique is able to build up time-frequency representation of an input signal with a great time and frequency resolution [18]. The *CWT* coefficients $W_{\Psi(a,b)}$ signal $\psi(n)$ at a scale $a(a > 0)$ and position b is expressed as follows [18].

$$W_{\Psi(a,b)} = \sum_{-\infty}^{\infty} \psi(n)\overline{\Psi}(\frac{n-b}{a}) \tag{8}$$

$\Psi(n)$ is a basis or mother wavelet with zero average and $\overline{\Psi}(n)$ is its conjugated values. *PSD* $P_{w(a,b)}$ of the *CWT* can be defined as follows

$$P_{W(a,b)} = |W_{\Psi(a,b)}|^2 \tag{9}$$

2) CLASSIFICATION

The output signal of the feature extraction block goes through the classification to separate the signal into different categories. There are many classifying techniques used to allocate signals into various groups. The most popular classifying techniques are support vector network (*SVM*), artificial neural network (*ANN*), hidden Markow models (HMM), fuzzy logic (FL), linear discriminant(*LN*), decision tree (*DTree*), Bayesian classifier (*BC*) and K- nearest neighbor (*KNN*) [19]. In these, *SVM* is kernel-based access and quite popular for non-linear data [19]. *KNN* is primarily acknowledged for the pattern-recognition approach [20]. Therefore, in this study *SVM*, *DTree* and *KNN* are employed to classify the breathing pattern of people.

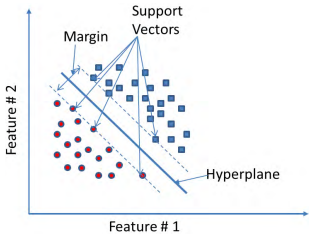

FIGURE 5. Linear support vector illustration.

a: SVM

Support Vector Machines (*SVM*) is a supervised machine learning algorithm which is used for both regression and classification problem. The main concept of *SVM* is to find the optimum decision boundary to separate two classes [21]. This decision boundary (hyperplane) maximize the margin between different classes. In *SVM*, support vectors are the data points nearest to the hyperplane that help in obtaining the optimal position of the hyperplane. The hyperplane, margin support vectors for classification problem are demonstrated in Fig. 5. In this figure, two features are chosen to apply *SVM* algorithm. The problem to separate different classes becomes finding an optimized hyperplane. The hyperplane decision function for binary problem is:

$$f(x) = sign\left(\sum_{i=1}^{N} a_i y_i K(x_i, x) + b\right) \tag{10}$$

where C is a penalty parameter, which regulates the trade-off between the imposed margins and allowed training error. represents Lagrange multipliers and is given as $0 \leq \alpha^i \leq C$ and $i = 1, 2, N$. The Kernel function is represented as $K(x_i, x)$ and x_i are the support vectors. Multi-class *SVM* can be generated using binary *SVMs*.

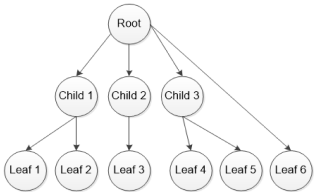

FIGURE 6. Decision tree model.

b: DECISION TREES

Similar to *SVMs*, Decision tree (*DT*) is one of vigorous algorithm. *DTs* have a tree-like structure, is simple and close to logical thinking of human. The *DT* is a crucial element of Random Forest - the most compelling algorithm nowadays [22], [23]. The *DT* model consists of different types of nodes as mentioned in Figure. 6. The starting node is called a root node, the internal nodes are the set of nodes *Child*1 to *Child*3, bottom nodes are class labels or leaf nodes. [24] In the *DT* model, to construct a reasonably good tree and to define attributes for each root note, *Grini impurity* (cost function) is given as follows: [24].

$$G(i) = 1 - \sum_{k=1}^{n} p_{i,k}^2 \tag{11}$$

where $G(i)$ is the *Gini* score of i^{th} node, $p_{i,k}$ is ratio between class k instances and training instance of i^{th} node. In the two-class problem, the best separation is achieved when $G(i) = 0$.

Another alternative to determine the cost function is to calculate the Entropy ($H(i)$) as follows.

$$H(i) = -\sum_{k=1}^{n} p_{i,k} log\left(p_{i,k}\right); \quad p_{i,k} \neq 0 \tag{12}$$

Both methods, Entropy and Gini impurity tend to point to analogous trees. There is not a big variation between two methods.

c: K NEAREST NEIGHBORS

K nearest neighbors (*KNN*) is called a lazy algorithm that stores all established vectors and class label correlated with each vector and classifies new cases based on a similarity measurement. This algorithm is widely used for practical problems [25], [26] *KNN* was first mentioned in $1970's$ as a non-parametric method [27]. In the *KNN*, the input vector is classified/ prediction by determining the similarity between this vector and the training instances (neighbors). Distance functions are used to measure the similarity between a new sample and the training data set. Those distance functions are Euclidean, Manhattan, Minkowski, and Hamming distance. The data used in *KNN* should be rescaled before processing to achieve a high accuracy result [28].

III. EXPERIMENT AND DATA

A. MEASUREMENT SET UP

The laboratory equipment - $N5244A\ PNA - X$ Microwave Network Analyzer plays a role of radar sensor system.

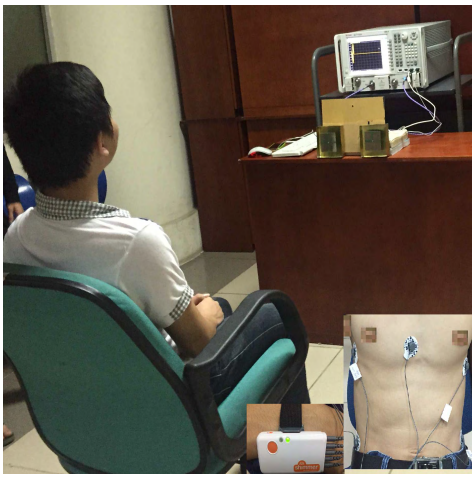

FIGURE 7. Measurement set up.

The internal transmitter and receiver of $N5244A\ PNA-X$ are utilized for this application. Two antennae are connected to two ports (transmitting and receiving ports) of $N5244A\ PNA-X$. A volunteer is sat in front of antennae as shown in Figure. 7, the distance from the antennae to the human position is 1 m. The transmitting power is $-8\ dBm$, the operating frequency is 1.6 Ghz, and the sampling frequency is 256 Hz. The same sampling frequency is set for a reference five-point touching Shimmer sensor.

Thirty one able-bodied participants (20 males and 11 females, average age 25.4 years) completed three sessions, each of which was approximately six minutes in duration. All sessions occurred on the same day with three minutes break between each session. The procedure of each session is described in Figure. 8. In the first session, participants were asked to breathe at their normal rate (i.e. 0.2 to 0.33 Hz) while in the remaining two sessions they were instructed to breathe at high ($>$ 0.33 Hz) and low ($<$ 0.2 Hz) rates respectively. Participants provided written informed consent, and the experiment was approved by the Head of School of Electronics and Telecommunications, Hanoi University of Science and Technology, Vietnam. The breathing rate of four random participants was measured by touching-probe Shimmer sensor at the same time they were measured by the remote sensor system to check the accuracy of the remote sensor. The remaining participants were only measured by the remote sensor to make sure that the natural signals were obtained.

TABLE 1. Data set description.

Data Sets No. of Subjects: 31 | Sampling Freq.: 256 Hz	Segmentation (in seconds)	Trial Size	Train	Test
Data set I	60	15360	348	117
Data set II	30	7680	697	233
Data set III	15	3840	1395	465

B. DATA SETS

The five-minute data for each individual per session was slotted into one minute, thirty seconds, and fifteen seconds recording. Based on the different segment length, three data sets were built as shown in Table 1.

- Data set I: From each individual, we get 15 data samples belonging to low, high and normal (5 for each category). Each data sample has 15360 data points($60\ sec \times 256\ Hz$ sampling rate). Total data set size is 465×15360 having 465 cases of all categories.
- Data set II: Similarly, 30 data samples are obtained from each person and the total data set size is 930×7680
- Data set III: This data set has the highest time resolution (15 seconds in each segmentation). The size of data set III is 1860×3840

Data sets are labeled into three categories low, high and normal. Spectral density in the frequency band from 0.1 Hz to 2 Hz is used as a feature. After feature extraction, the data set was divided into two sets 75% for the training set and 25% for the testing set. The size of train and testing sets in each data set is displayed in Table 1. To avoid the over fitting problem, 10×10 fold cross validation is used for the classification of the training set.

C. EVALUATION METRIC

In this paper, classification accuracy is unsterilized as an evaluation metric. The accuracy in the three classifications case can be determined as follows.

$$Accuracy = \frac{P_{cr}}{P_{cr} + P_{Icr}} \tag{13}$$

where

- P_{cr} is the number of correct predictions.
- P_{Icr} is the number of incorrect predictions.

IV. RESULTS

The measured breathing rate by remote radar sensor system in time and frequency domains are displayed in Figure. 9 and Figure. 10.

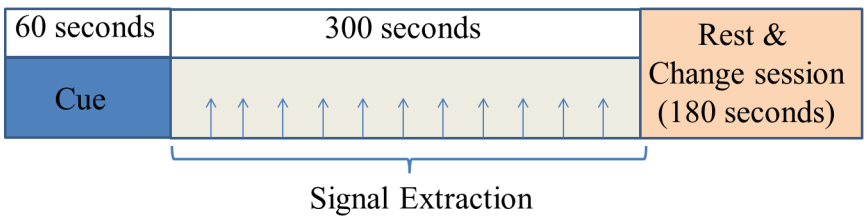

FIGURE 8. Experimental procedure.

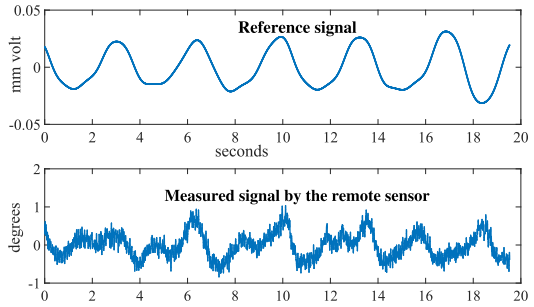

FIGURE 9. Measured signal in the time domain.

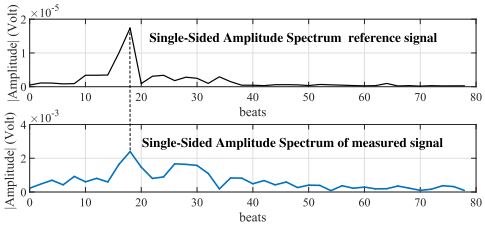

FIGURE 10. Measured signal in the frequency domain.

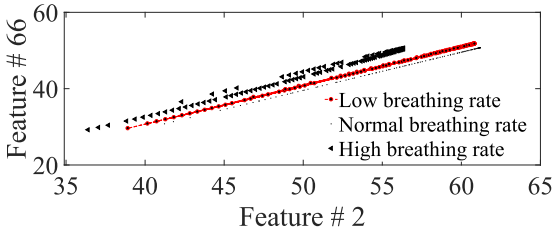

FIGURE 11. Relation between feature # 2 and feature # 66 in the data set I.

The frequency domain signal can give the respiratory rate of a person. In this approach, the corresponding frequency at the highest absolute magnitude of spectrum is considered as breathing frequency. This technique is called peak position detection [29]. The absolute spectrum of each segment signal can be calculated by *STFT* as shown in Figure. 10. Figure. 10 gives the breathing rate of 18 *beats*/*minute*, the signal from remote sensor is coincided with the signal from the reference touching sensor. From both Figures, one can see that the remote sensor system introduces more noise than the touching sensors, however, the remote radar sensor gives a similar result of breathing rate to the five- probes Shimmer sensor.

Figure 11 and Figure 12 illustrate the relationship between two features in the feature vector of data set I and data set III. It is clear that in data set I (Figure 11), three classes are separated properly, while in Figure 12, there are some overlaps between classes. This phenomena come from time resolutions of each data set. Data set I has the lowest time resolution (60 seconds segmentation), while data set III has the highest time resolution (15 seconds segmentation). The increase in time resolution is compensated to the accuracy of the system as mentioned in Table2.

Table 2 compares the accuracy of the proposed remote sensing system in classifying breathing rate problems into

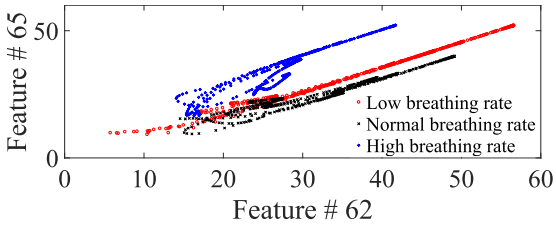

FIGURE 12. Relation between feature # 62 and feature # 65 in the data set III.

three categories (fast, normal, and slow) with the conventional method (based on peak position detection). Different classifying techniques are applied and results are shown in Table. 2. From this Table, we can see that data set I gives very good results (above 99%) with *KNN* and *SVM* classifiers. *DTree* introduces lower accuracy (around 95%). In data set II, the segmentation is half of segmentation in the data set I. However, *SVM* and *KNN* classifications still introduce similar results under *CWT* and *STFT* extraction methods. For *DTree* with *CWT* extraction method, the accuracy is similar to the data set *I*. There is a large reduction (14%) accuracy under *DTree* classifier when feature are selected by *STFT*. When the segmentation of data reduce to the size of 15 *seconds* in the data set III, the accuracies of the system under *SVM* and *KNN* techniques does not change much. Notwithstanding, *DTree* delivers a significant reduction of accuracy. In *DTree* method, under *STFT* and *CWT* extraction methods, the accuracies of test set III are 75.81% and 83.01% respectively.

The conventional method introduces lower results, for data set *I* and *II* the results are comparable with the recent work [30]. The accuracy of modified *STFT* in reference [30] is around 80% while our results are around 64%. There are several reasons behind that difference. Firstly, the transmitting power of their system was eight times our transmitting power. Their system operated at much higher frequency (around 24 *GHz*) while the proposed system operated at 1.6 *GHz*. The result is that our system is less sensitive than their system fifteen times.

The length of segmentation has a significant effect on the accuracy of breathing rate estimation when the peak position detection method is used. As discussed in the reference [31], this method introduces high accuracy when the segmentation is larger than 60 seconds. Data set III introduces very low accuracy (35.48%) because of the low frequency resolution. In this data set, 15 seconds' observation window corresponds to $1/15 = 0.067\,Hz$ frequency resolution. This frequency resolution equals to 4.02 beats/min, therefore, the peak position detection methods shows very poor result (just 35.48%).

Generally, The *CWT* extraction technique presents better results than *STFT*. The performance of machine learning based methods outperforms the conventional method (peak position detection) because our proposed system used the whole *CWT* or *STFT* vector (including peak spectral and its harmonics) for classification while the conventional method use only one element (peak spectral). The result in Table 2 gives a good suggestion for further applications.

TABLE 2. Classification accuracy of proposed system.

Data Sets	Extraction methods	Classification Methods			Conventional method (Peak position detection)
		SVM	DTree	KNN	
Data set I	STFT	99.89 %	94.51%	99.11 %	64.09 %
	CWT	99.95 %	96.58 %	99.88 %	
Data set II	STFT	99.85 %	80.68 %	99.15 %	63.76 %
	CWT	99.87 %	96.13 %	99.45 %	
Data set III	STFT	99.12 %	75.81 %	99.11 %	35.48 %
	CWT	99.67 %	83.01 %	99.55 %	

V. CONCLUSION AND FUTURE WORK

From measured results, the remote radar sensor system can accurately capture breathing rate, and is more comfortable for the measured person. The remote radar sensor system has high potential in informing the user of their instantaneous breathing rate by the *TF* feature extraction techniques. Moreover, the *AI* technique that was applied on the data obtained by the remote radar sensor system, makes this system smarter and gives useful information to the end user. The aim of the proposed machine learning model is to classify the measured signal from the radar sensor system in different categories. This model is then integrated with the radar sensor system and gives a warning to people, for instance, if their breathing rate is abnormal. The accuracy of our proposed approach is far greater than the conventional method. The *SVM* and *KNN* classifications gave good accuracy on three types of data sets of 31 measured people. The measurement results suggest an alternative high accuracy method in category three types breathing rate.

The results of this research show the high potential application of remote radar sensor in diagnosing complicated breathing/sleeping disorder problems. The system might give high accuracy results because the sleep pattern of patients can be measured remotely. The measuring system will provide a comfortable environment for patients. The next step of this work is to collect data from breathing disorder patients. The model is then developed to recognize different types of sleeping disorder like untreated central sleep appoea, Cheyne Stokes, dysrhythmic breathing and so on.

REFERENCES

[1] C. G. Caro and J. A. Bloice, "Contactless apnoea detector based on radar," *Lancet*, vol. 298, no. 7731, pp. 959–961, Oct. 1971.

[2] T. E. McEwan, "Body monitoring and imaging apparatus and method," U.S. Patent 5 573 012, Nov. 12, 1996.

[3] C. G. Bilich, "Bio-medical sensing using ultra wideband communications and radar technology: A feasibility study," in *Proc. Pervasive Health Conf. Workshops*, Nov./Dec. 2006, pp. 1–9.

[4] E. Cianca and B. Gupta, "FM-UWB for communications and radar in medical applications," *Wireless Pers. Commun.*, vol. 51, no. 4, pp. 793–809, Dec. 2009.

[5] D. Zito *et al.*, "SoC CMOS UWB pulse radar sensor for contactless respiratory rate monitoring," *IEEE Trans. Biomed. Circuits Syst.*, vol. 5, no. 6, pp. 503–510, Dec. 2011.

[6] S. Pisa, E. Pittella, and E. Piuzzi, "A survey of radar systems for medical applications," *IEEE Aerosp. Electron. Syst. Mag.*, vol. 31, no. 11, pp. 64–81, Nov. 2016.

[7] C. Gu, Z. Peng, and C. Li, "High-precision motion detection using low-complexity doppler radar with digital post-distortion technique," *IEEE Trans. Microw. Theory Techn.*, vol. 64, no. 3, pp. 961–971, Mar. 2016.

[8] C. Li *et al.*, "A review on recent progress of portable short-range noncontact microwave radar systems," *IEEE Trans. Microw. Theory Techn.*, vol. 65, no. 5, pp. 1692–1706, May 2017.

[9] C. Will *et al.*, "Local pulse wave detection using continuous wave radar systems," *IEEE J. Electromagn., RF Microw. Med. Biol.*, vol. 1, no. 2, pp. 81–89, Dec. 2017.

[10] J. Muehlsteff, "Method and apparatus for monitoring the respiration activity of a subject," U.S. Patent 9,883,821, Feb. 6 2018.

[11] Y. S. Lee, P. N. Pathirana, and C. L. Steinfort, "Respiration rate and breathing patterns from doppler radar measurements," in *Proc. IEEE Conf. Biomed. Eng. Sci. (IECBES)*, Dec. 2014, pp. 235–240.

[12] G. Yuan, N. A. Drost, and R. A. McIvor, "Respiratory rate and breathing pattern," *McMaster Univ. Med. J.*, vol. 10, no. 1, pp. 23–25, Nov. 2013.

[13] N. T. Van Phuoc, L. Tang, S. C. Mukhopadhyay, D. M. Nguyen, and F. Hasan, "Probabilities of false alarm for vital sign detection on the basis of a doppler radar system," *Sensors*, vol. 18, no. 3, p. 694, Feb. 2018.

[14] Z. Yu, D. Zhao, and Z. Zhang, "Doppler radar vital signs detection method based on higher order cyclostationary," *Sensors*, vol. 18, no. 1, p. 47, Dec. 2017.

[15] H. Zhao, H. Hong, L. Sun, Y. Li, C. Li, and X. Zhu, "Noncontact physiological dynamics detection using low-power digital-IF doppler radar," *IEEE Trans. Instrum. Meas.*, vol. 66, no. 7, pp. 1780–1788, Jul. 2017.

[16] B. Boashash and S. Ouelha, "Efficient software platform TFSAP 7.1 and Matlab package to compute time–frequency distributions and related time-scale methods with extraction of signal characteristics," *SoftwareX*, vol. 6, pp. 48–52, Jul./Dec. 2017.

[17] J. M. D. Haan, "A survey on methods for time-frequency analysis," Dept. Signal Process., Blekinge Inst. Technol., Karlskrona, Sweden, Tech. Rep. oai:bth.se:arkivexC125660F002EA348C12568A3002CAB0A, 1998.

[18] J. B. Tary, R. H. Herrera, and M. van der Baan, "Analysis of time-varying signals using continuous wavelet and synchrosqueezed transforms," *Philos. Trans. Roy. Soc. A, Math., Phys. Eng. Sci.*, vol. 376, no. 2126, Aug. 2018, Art. no. 20170254.

[19] N. Nazmi, M. A. Abdul Rahman, S. Yamamoto, S. A. Ahmad, H. Zamzuri, and S. A. Mazlan, "A review of classification techniques of EMG signals during isotonic and isometric contractions," *Sensors*, vol. 16, no. 8, p. 1304, Aug. 2016.

[20] Y. Q. Chen, R. I. Damper, and M. S. Nixon, "On neural-network implementations of k-nearest neighbor pattern classifiers," *IEEE Trans. Circuits Syst. I. Fundam. Theory Appl.*, vol. 44, no. 7, pp. 622–629, Jul. 1997.

[21] C. Venkatesan, P. Karthigaikumar, A. Paul, S. Satheeskumaran, and R. Kumar, "ECG signal preprocessing and SVM classifier-based abnormality detection in remote healthcare applications," *IEEE Access*, vol. 6, pp. 9767–9773, 2018.

[22] H. Lan. (2017). *Decision Trees and Random Forests for Classification and Regression*. [Online]. Available: https://towardsdatascience.com/decision-trees-and-random-forests-for-classification-and-regression-pt-2-2b1fcd03e342

[23] A. Géron, *Hands-On Machine Learning with Scikit-Learn and TensorFlow: Concepts, Tools, and Techniques to Build Intelligent Systems*. Newton, MA, USA: O'Reilly Media, 2017.

[24] R. Rivera-Lopez and J. Canul-Reich, "Construction of near-optimal axis-parallel decision trees using a differential-evolution-based approach," *IEEE ACCESS*, vol. 6, pp. 5548–5563, 2018.

[25] Y. Bao, X. Du, M. Deng, and N. Ishii, "An efficient method for computing all reducts," *Trans. Jpn. Soc. Artif. Intell.*, vol. 19, no. 3, pp. 166–173, 2004.
[26] W. Wu, J. Liu, H. Rong, H. Wang, and M. Xian, "Efficient k-nearest neighbor classification over semantically secure hybrid encrypted cloud database," *IEEE Access*, vol. 6, pp. 41771–41784, 2018.
[27] E. A. Patrick and F. P. Fischer, III, "A generalized *k*-nearest neighbor rule," *Inf. Control*, vol. 16, no. 2, pp. 128–152, Apr. 1970.
[28] J. Brownlee. (2016). *K-Nearest Neighbors for Machine Learning*. [Online]. Available: https://machinelearningmastery.com/k-nearest-neighbors-for-machine-learning/
[29] A. Tariq, "Vital signs monitoring using doppler radar and on-body antennas," Ph.D. dissertation, School Electron., Elect. Comput. Eng. College Eng. Phys. Sci., Univ. Birmingham, Birmingham, U.K., 2013.
[30] M. Mabrouk, S. Rajan, M. Bolic, M. Forouzanfar, H. R. Dajani, and I. Batkin, "Human breathing rate estimation from radar returns using harmonically related filters," *J. Sensors*, vol. 2016, Jan. 2016, Art. no. 9891852.
[31] A. Gunasekara, "Contactless estimation of breathing rate using UWB radar," Ph.D. dissertation, Inst. Elect. Comput. Eng., School Elect. Eng. Comput. Sci., Univ. Ottawa, Ottawa, ON, Canada, 2017.

NGUYEN THI PHUOC VAN received the B.Sc. degree in telecommunication engineering from the Hanoi University of Communication and Transport, Vietnam, in 2001, and the M.Sc. degree in electronics and information technology from Vrije University Brussel, Belgium, in 2013. She is currently pursuing the Ph.D. degree with the School of Engineering and Advance Technology, Massey University, New Zealand. She was with the Hanoi University of Industry, Hanoi, Vietnam. She is involved in the Doppler radar sensing systems for vital signs detection. Her research interests include vital signs sensing systems, sensing technology for monitoring the human health care condition, and rescuing purpose.

LIQIONG TANG received the Ph.D. degree from the University of Liverpool, U.K. She started the Mechatronics Program at Massey University and was the Cluster Leader of the Mechatronics Program for over ten years. With her leadership, the Mechatronics Program becomes one of the most active programs at Massey University. She has been involved in a number of research projects in industry, healthcare, and defense force and constantly received research funding from industry and major funding bodies, such as National Science Challenge and Callaghan Innovation. She has served as an Accessor for major science and technology funding bodies and a Board Member/Reviewer for international journals in robotics and mechatronics. She has been with Massey University, since 1996, where she is currently the Deputy Director of the Postgraduate Programs in the School of Engineering and Advanced Technology. Her research interests include robotics, mechatronics, intelligent control, and industrial automation.

AMARDEEP SINGH received the M.Sc. degree in computer science and the Engineering degree from the Guru Nanak Dev University, in 2013. He is currently pursuing the Ph.D. degree with the School of Fundamental Sciences, Massey University. His fields of interest include brain–computer interface and machine learning.

NGUYEN DUC MINH received the Ph.D. degree in electrical engineering from the University of Kaiserslautern, Germany, in 2009, where he was a Scientific Staff Member. He is currently an Associate Professor with the School of Electronics and Telecommunications, Hanoi University of Science and Technology, Vietnam. His research activities involve digital signal processing design, embedded system design, formal verification of digital design, and embedded systems.

SUBHAS CHANDRA MUKHOPADHYAY (M'97–SM'02–F'11) graduated from the Department of Electrical Engineering, Jadavpur University, Calcutta, India, with a Gold medal. He received the master's degree in electrical engineering from the Indian Institute of Science, Bengaluru, India, the Ph.D. (Eng.) degree from Jadavpur University, and the Dr. Eng. degree from Kanazawa University, Japan. He is currently a Professor of mechanical/electronics engineering with the Department of Engineering, Macquarie University, NSW, Australia. He is also the Program Leader of the Mechatronics Engineering Degree Program. He has over 26 years of teaching and research experiences. He has authored/co-authored over 400 papers in different international journals, conferences, and book chapters. He has edited 15 conference proceedings. He has also edited 17 special issues of international journals as a Lead Guest Editor and 30 books with Springer-Verlag. His fields of interest include smart sensors and sensing technology, wireless sensor networks, instrumentation and measurements, the Internet of Things, environmental measurements, electromagnetics, control engineering, mechatronics, magnetic bearing, fault current limiter, electrical machines, and numerical field calculation. He is a Fellow of the IET (U.K.) and the IETE (India). He was awarded numerous awards throughout his career and attracted over U.S.$3.0 M on different research projects. He has delivered 296 seminars, including keynote, tutorial, and invited and special seminars. He is a Topical Editor of the IEEE Sensors Journal and an Associate Editor of the IEEE Transactions on Instrumentation and Measurements. He is in the Editorial Board of the *e-Journal on Non-Destructive Testing*, *Sensors and Transducers*, and the *Transactions on Systems, Signals and Devices*. He is the Co-Editor-in-Chief of the *International Journal on Smart Sensing and Intelligent Systems*. He was the Technical Program Chair of ICARA 2004, ICARA 2006, ICARA 2009, and the IEEE I2MTC 2016. He was the General Chair/Co-Chair of ICST 2005, ICST 2007, the IEEE ROSE 2007, the IEEE EPSA 2008, ICST 2008, the IEEE Sensors 2008, ICST 2010, the IEEE Sensors 2010, ICST 2011, ICST 2012, ICST 2013, ICST 2014, ICST 2015, and ICST 2016. He has organized the IEEE Sensors Conference 2009 at Christchurch, New Zealand, in 2009, as the General Chair. He has organized the 11th ICST in Sydney, Australia, in 2017. He is the Ex-Chair of the IEEE Instrumentation and Measurement Society New Zealand Chapter. He is a Distinguished Lecturer of the IEEE Sensors Council, from 2017 to 2019.

SYED FARAZ HASAN received the bachelor's degree in electrical engineering from the NED University of Engineering and Technology, Pakistan, in 2008, and the Ph.D. degree from the University of Ulster, U.K., in 2011. He was with Sungkyunkwan University, South Korea, and the Korea Advanced Institute of Science of Technology (KAIST). He is currently with the School of Engineering and Advanced Technology, Massey University, New Zealand, where he leads the Telecommunication and Network Engineering Research Group. His research interests include device-to-device communication, energy harvesting, and localization techniques.